TECHNICAL MEMORANDUM

297

Tropical singular vectors computed with linearized diabatic physics

J. Barkmeijer, R. Buizza, T.N. Palmer,
K. Puri and J-F. Mahfouf

Research Department

December 1999

European Centre for Medium-Range Weather Forecasts
Europäisches Zentrum für mittelfristige Wettervorhersage
Centre européen pour les prévisions météorologiques à moyen

Abstract

With the introduction of diabatic processes in the forward and adjoint tangent models of the European Centre for Medium-Range Weather Forecasts' model, it is possible to determine singular vectors (SVs) for situations where diabatic physics may be important in producing perturbation growth. In this paper, the linear physical parametrizations are used to compute SVs for the tropical region, or subsets thereof, with an optimization time of 48 h. Perturbation growth is measured in terms of the so-called total energy norm, augmented with a term for specific humidity.

Difficulties that may arise in computing tropical SVs, such as associated with spurious upper-tropospheric perturbation growth are described. Also the impact on the SV structure by including a specific humidity term in the defining norm is discussed. Using a term for specific humidity based on background error statistics in the norm at initial time yields SVs with a more realistic specific humidity vertical profile.

SVs are determined in various configurations for two tropical cyclones. Results show that targeting in the vicinity of the cyclone is required to obtain SVs associated with the cyclone dynamics. The dominant targeted SVs for tropical cyclones show resemblance to fast-growing structures found for idealized vortices.

1 Introduction

Numerical weather prediction (NWP) models describe an intricate balance between different components of the equations of climate such as dry advective dynamics and diabatic processes like condensation and moist convection. As a consequence, the error growth properties of a NWP model are strongly influenced by how these processes interact. Studies of the intrinsic growth of forecast errors, considering the evolution of differences between consecutive forecasts yield error-doubling times of about 1.5 to 2 days (e.g., Lorenz, 1982; Simmons et al., 1995). By computing so-called sensitivity fields (Rabier et al., 1996) or pseudo inverses of the forecast error (Gelaro et al., 1998), it is possible to identify fast-growing components of the analysis error. The largest possible error growth in terms of a suitable error norm during a fixed forecast period can, in principle, only be found by solving a nonlinear optimization problem. In practice, it is assumed that error growth is linear for say 2 days. Then the nonlinear optimization problem reduces to an eigenvalue problem for which efficient solvers, e.g. the Lanczos algorithm (Parlett, 1980), exist.

Although the assumption of linear error growth simplifies the computation of fast growing structures, it still requires a linearized version of the forecast model together with its adjoint because of the large dimensionality of the model. Linear models have been developed first for the adiabatic part of the forecast model, using a simplified scheme for the vertical diffusion (Buizza, 1994). Although in that case the dynamics of the linear and nonlinear forecast model do not correspond precisely, they have been successfully used in various applications. In variational data assimilation, they are essential in determining the gradient of a cost function with respect to initial conditions (Thépaut and Courtier, 1991; Rabier et al., 1997). They are also needed in the computation of singular vectors which are used in ensemble prediction systems to create initial perturbations (Buizza and Palmer, 1995; Molteni et al., 1996).

Recently, linear models including moist physical processes have been developed. There is not an obvious strategy to include physical processes in the linear models, because of strong nonlinearities and the frequent dependence on logical conditionals in these processes. For a regional mesoscale model, the accuracy of the diabatic linearization is described in Vukićević and Errico (1993) and more recently in Errico and Reader (1998). They show that the accuracy depends on the atmospheric situation. Generally speaking, the match between the linear and nonlinear integrations is better over regions where geostrophically-balanced dynamics is more important than over regions dominated by convective processes. In their approach, perturbations are given a magnitude comparable to analysis uncertainties. Investigating the validity of the linear approximation in such a way is important from a practical point of view, because it reflects the actual use of singular vectors in ensemble prediction systems. Ehrendorfer et al. (1999) describe the impact of moist physics on properties as growth rate of extra-tropical singular vectors. Inclusion of diabatic processes in the linear models creates new possibilities for SVs to produce perturbation growth.

In this paper the linearized physics package of the European Centre for Medium-range Weather Forecasts' (ECMWF) global model as presented in Mahfouf (1999) is used to compute singular vectors. In particular, the singular vectors are targeted for the tropics (or subsets thereof) as defined by the longitudinal band 30°S - 30°N. This area is not yet sampled in the current ECMWF ensemble prediction system, because the simplified physics currently used in the singular vector computation (Buizza, 1994) is not suitable to describe the physical processes in the tropics. The goal of the paper is to investigate the impact of moist physics on the tropical singular vector structure and thereby to isolate and reduce possible spurious growth mechanisms in the linearized model. In a companion paper (Puri et al., 1999) the impact of targeted tropical singular vectors, associated with tropical cyclones, on the performance of the ECMWF Ensemble Prediction System (EPS) will be studied.

In defining singular vectors, one always faces the problem of selecting an appropriate norm to measure perturbation growth. The choice of norm depends on the particular application. For example, in case of forecast error covariance prediction, a norm at initial time based on the analysis error covariance matrix is the most appropriate (Ehrendorfer and Tribbia, 1997; Palmer et al, 1998; Barkmeijer et al., 1998). In this study we consider the total energy norm augmented by a term measuring specific humidity as used in Mahfouf et al. (1996), Buizza et al. (1996) and Ehrendorfer et al. (1999). We also experimented with a specific humidity norm based on error variances as used in the background error covariance matrix, operationally used at ECMWF (Derber and Bouttier, 1999).

In section 2 we briefly outline the model and linearized physics used in the singular vector computation. Singular vectors and norms are defined in section 3. In section 4 examples and properties of tropical singular vectors are given for various settings, such as choices of the norm and target area. Special attention is given to an undesirable feature of the linearized model in creating linearly fast-growing upper-tropospheric structures which are damped in the nonlinear forecast model. Section 5 is on tropical singular vectors targeted for tropical cyclones. The results are summarized in Section 6.

2 The model and synoptic situations

The model used in this study is a low resolution version of the ECMWF global spectral model with 31 vertical levels. In computing singular vectors the nonlinear model and both the linear and adjoint versions are integrated with an Eulerian advection scheme with a 20 minute time step and a triangular truncation at wavenumber 42. The chosen optimization time of the singular vectors is 48 hours. The linearized physics is the same as described in Mahfouf (1999) and

comprises vertical diffusion, subgrid-scale orographic effects, large scale condensation, longwave radiation and deep cumulus convection. Integrations with finite size perturbations (analysis increments) have shown that the fit between the linear and nonlinear model (using all physics) improves when physics is included in the linear model. This set of linear parametrizations is currently used in the operational ECMWF 4D-Var assimilation system (Mahfouf and Rabier, 1999). Inclusion of physical processes increases the computational cost of singular vectors considerably. Apart from more memory to store additional fields during the nonlinear integration, the required computing time increases by a factor of 6.

Tropical singular vectors targeted for the entire tropical strip were studied for two cases with forecasts starting from 7 February 1997 12 UTC (winter case) and from 2 July 1997 (summer case). Also singular vectors were computed for two tropical cyclones. The selected cyclones were Bonnie in the Atlantic area and Zeb in the Pacific area, with forecasts starting from 19 August 1998 12 UTC and 11 October 1998 12 UTC respectively.

3 Singular vectors and norms

When linear perturbation growth is assumed during a certain forecast time, fast-growing structures or singular vectors (SVs) can be determined by solving an eigenvalue problem (Lorenz, 1965). Apart from an optimization time, during which perturbation growth is considered (in this study 48 hours), it is necessary to specify a norm both at initial and optimization time to measure perturbation growth. Given such norms $\mathbf{E}_0$ and $\mathbf{E}_1$, which are defined below, singular vectors $\mathbf{x}$ maximize the following ratio:

$$\frac{\langle \mathbf{PMx}, \mathbf{E}_1\mathbf{PMx} \rangle}{\langle \mathbf{x}, \mathbf{E}_0\mathbf{x} \rangle} \tag{1}$$

Here $\langle\ ,\ \rangle$ denotes the Euclidean inner product $\langle \mathbf{x}, \mathbf{y} \rangle = \sum \mathbf{x}_i\mathbf{y}_i$ and $\mathbf{M}$ is the propagator of the tangent model valid for the optimization time. The positive definite and symmetric operators $\mathbf{E}_0$ and $\mathbf{E}_1$ induce a norm at initial and final time respectively. The operator $\mathbf{P}$ is a projecting operator setting a vector to zero outside a given domain, e.g. outside the band 30°S - 30°N. The first singular vector SV1 maximizes the ratio in eq. 1, the second singular vector SV2 maximizes this ratio in the subspace $\mathbf{E}_0$-orthogonal to SV1, and so forth. Thus the singular vectors $\mathbf{x}$ define an $\mathbf{E}_0-$orthogonal set at initial time. The evolved singular vectors $\mathbf{Mx}$ form an $\mathbf{E}_1-$orthogonal set at optimization time in the domain defined in $\mathbf{P}$. Alternatively, these singular vector are solutions of the following generalized eigenvalue problem

$$\mathbf{M}^\star\mathbf{P}^\star\mathbf{E}_1\mathbf{PMx} = \lambda\mathbf{E}_0\mathbf{x} \tag{2}$$

The adjoint operators $\mathbf{M}^\star$ and $\mathbf{P}^\star$ are defined with respect to the Euclidean inner product. For $\mathbf{E}_0$ in the form of a diagonal matrix, as is the case for the norms considered in this paper, the square root of $\mathbf{E}_0$ is readily determined. Multiplying both sides of (2) to the left and right with the inverse of the square root of $\mathbf{E}_0$, allows us to reduce (2) to an ordinary eigenvalue problem. Although the operators $\mathbf{S}$ in (2), with $\mathbf{S}$ being $\mathbf{M}$, $\mathbf{P}$, $\mathbf{E}_0$ and $\mathbf{E}_1$, are not known explicitly, it is possible to evaluate $\mathbf{Sy}$ for a given input $\mathbf{y}$. This suffices for eigenproblem solvers as the Lanczos algorithm, see e.g. Parlett (1980), to compute solutions of (2) in an efficient manner.

The norms $\mathbf{E}_0$ and $\mathbf{E}_1$ considered in this study are extensions of the so-called (dry) total energy (TE) norm, which is used at ECMWF to compute singular vectors for the Ensemble Prediction System (Buizza and Palmer, 1995). The only difference is an additional term which measures specific humidity q. One of the norms we will consider is the moist TE-norm of which the associated innerproduct reads as:

$$\begin{aligned}\langle \mathbf{x}, \mathbf{Ey} \rangle &= \frac{1}{2}\int_0^1 \int_\Sigma (\nabla\Delta^{-1}\zeta_x \cdot \nabla\Delta^{-1}\zeta_y + \nabla\Delta^{-1}D_x \cdot \nabla\Delta^{-1}D_y \\ &+ \frac{c_p}{T_r}T_x T_y + w_q \frac{L_c^2}{c_p T_r} q_x q_y) \mathrm{d}\Sigma (\frac{\partial p}{\partial \eta}) \mathrm{d}\eta + \frac{1}{2}\int_\Sigma R_d T_r P_r \ln \pi_x \cdot \ln \pi_y \mathrm{d}\Sigma \end{aligned} \quad (3)$$

with $(\zeta_x, D_x, T_x, q_x, \ln \pi_x)$ being the vorticity, divergence, temperature, specific humidity and logarithm of the surface pressure components of the state vector $\mathbf{x}$ and c_p is the specific heat of dry air at constant pressure, $p(\eta)$ the pressure at eta levels (0 = surface and 1 = top of atmosphere), R_d is the gas constant for dry air, $T_r = 300$ K is a reference temperature, $P_r = 800$ hPa is a reference pressure, L_c is the latent heat of condensation and w_q is a constant.

The norm without the $q-$term will be referred to as the dry TE-norm. The choice for the weights of the $q-$component of the state vector in the moist TE-norm is motivated by the interaction between moisture and temperature in the linearized condensation process. The linearized large-scale condensation scheme has the property (Mahfouf, 1999) that the temperature T and specific humidity q of a perturbation satisfy $c_p T = -L_c q$. Consequently, the temperature term in (3) can be written as $c_p^2 T_x T_y/(c_p T_r) = L_c^2 q_x q_y/(c_p T_r)$. The latter expression is simply added to the dry TE-norm to define the moist TE-norm. Note that there is a weighting factor w_q in the $q-$term. In the extreme case of $w_q \gg 1$, the dry fields will dominate at initial time, while at final time the specific humidity field will dominate (vice versa for $w_q \ll 1$). To ensure that all components of the state vector contribute to the norm in the SV computation, both at initial and final time, a moist TE-norm with $w_q = 1$ was used, following Buizza et al. (1996), Mahfouf et al. (1996) and Ehrendorfer et al. (1999). This value proved to be a suitable choice for the computation of extra-tropical SVs. For later reference we denote SVs computed with the new linearized physics and the dry or moist TE-norm both at initial and final time by new0 and new1 respectively. When the linearized physics is used with the simplified vertical diffusion

scheme as described in Buizza (1994), the SVs are referred to as old1 and old0 depending on whether the moist TE-norm is used or not respectively. Observe that even with simplified physics SVs may generate energy in specific humidity simply through advection from the basic state.

We also experimented with an alternative term for specific humidity q in the moist TE norm by using background error statistics for q. For this we used for each model level the average error variances for q, averaged over total wavenumbers, as they are specified for the operational ECMWF background error covariance matrix (Derber and Bouttier, 1999). The inverse of these averaged error variances, multiplied by a suitable factor, defines the new q weights in the modified moist TE-norm. With a multiplication factor of 5.0, the two versions of q weights are comparable for the lower part of the atmosphere; above model level 18 (500 hPa) the new q weights increase strongly. See Fig 1 for the two versions of q weights with respect to model levels.

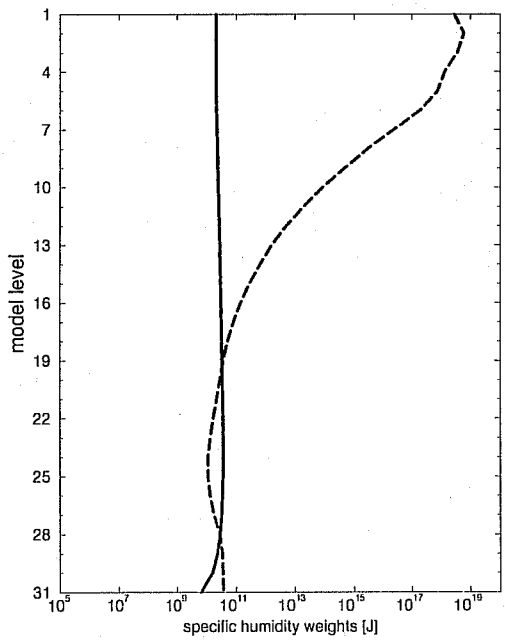

Figure 1: *Weights for specific humidity as used in the standard (solid) and modified (dashed) moist total energy norm.*

4 Results

We first present tropical SVs for forecasts starting from 7 February 1997 and 2 July 1997 both at 12 UTC. The optimization time used in the SV computation is 48 hours and the target area consists of the tropical band 30°S–30°N. Since the results for both the summer and winter case are often qualitatively quite similar we will mainly focus on the winter case hereafter.

Fig. 2 shows the vorticity fields of the leading SV of type new1 for the winter (left column) and summer (right column) case at model levels 10, 11 and 12 (around 208 hPa, 238 hPa and 270 hPa respectively) at initial time. The amplitude at other model levels is negligible. The singular vector (especially for the winter case) has a shallow structure with amplitude concentrated at a few model levels. This is confirmed by plotting the vertical distribution of the various components of the TE-norm as in Fig. 3 for SV1 (most of the leading SVs show a similar vertical profile).

The tropical SVs reveal a shallow structure which is entirely located in the upper-troposphere and dominated by the vorticity and divergence component. Buizza and Palmer (1995) also observed a similar tropical SV structure computed with the dry TE norm and simplified linearized physics. The vertical structure of the tropical SVs differs considerably from what is known of extra-tropical total energy SVs, where initially most of the energy is around 700 hPa.

Computing SVs for the different norms and using linear models with simplified and moist physics gives similar upper-tropospheric structures for the leading SVs of new0, old0 and old1 (see section 3 for definition). The possible differences between the various types of SVs may be quantified by determining the similarity index as in Buizza (1994). In the computation of the similarity index, the unstable subspaces spanned by the leading SVs of two sets are compared by projecting one set of SVs onto another. The mean of the projection coefficients is a measure of how much the two sets of SVs differ: it ranges from 0 (for orthogonal subspaces) to 1 (for identical subspaces). In order to compare the dry and moist SVs only the dry part of the moist SV and the dry TE-norm is used in determining the projection coefficients. The results for the summer and winter cases are presented in Table 1.

winter case	old0	old1	new0	new1	**summer case**	old0	old1	new0	new1
old0	1	.93	.61	.54	old0	1	.75	.56	.48
old1		1	.61	.53	old1		1	.54	.44
new0			1	.88	new0			1	.82
new1				1	new1				1

Table 1. *Similarity indices between unstable subspaces spanned by the 15 leading tropical SVs based on dry and moist norms (denoted by suffix 0 and 1 respectively) and with simplified and new physics.*

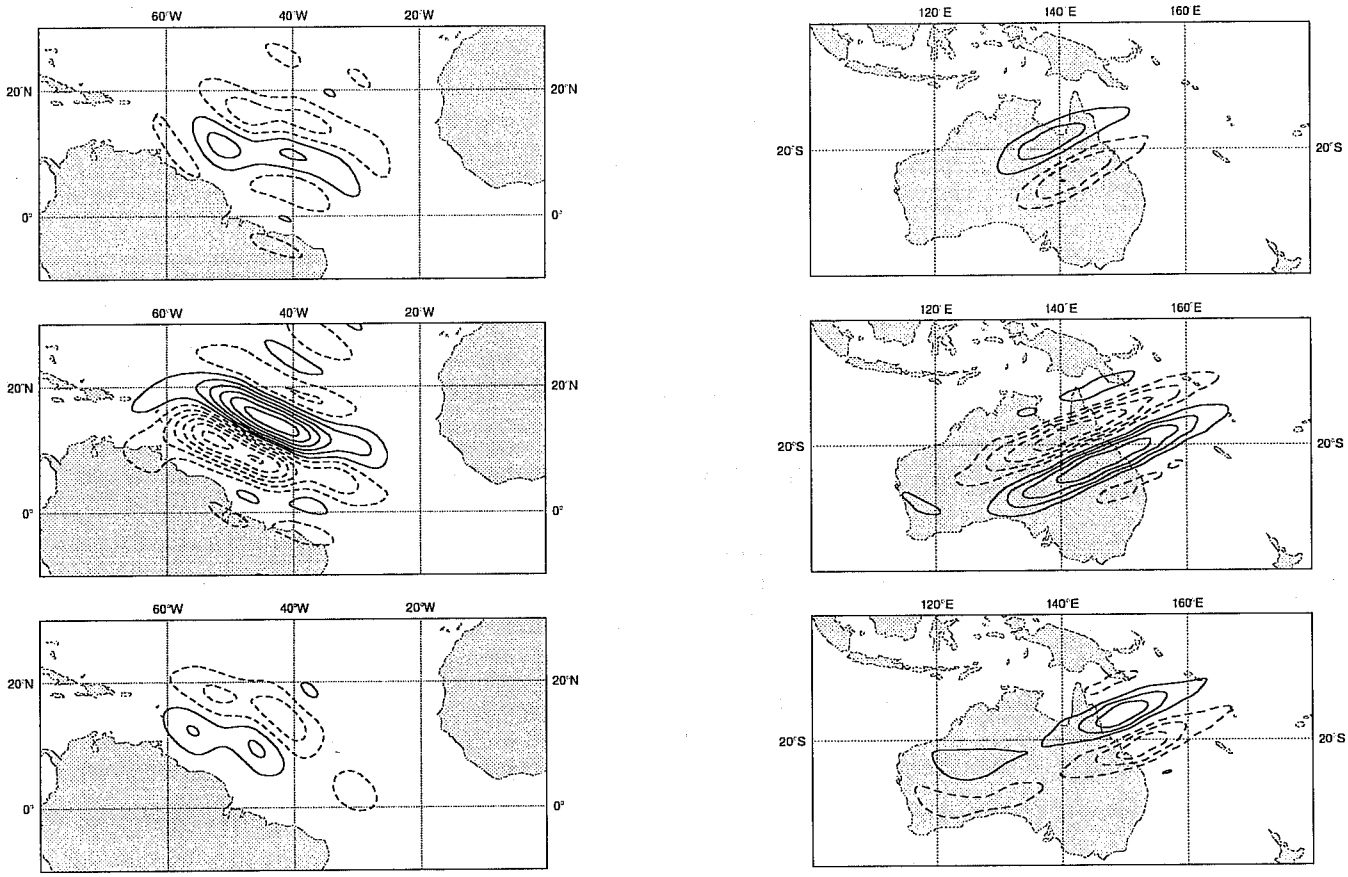

Figure 2: *Left column: vorticity field of SV1 for 7 February 1997 at model level 10, 11 and 12 (208 hPa, 238 hPa and 270 hPa respectively) from top to bottom panel. Right column: same but for 2 July 1997. All panels use the same contour interval; positive or negative values are given in solid or dashed contours respectively.*

The upper-tropospheric SVs, which have mainly energy in the vorticity and divergence component, dominate in all types of SVs. This explains the high similarity between old0/old1 and new0/new1. Inspection of the SVs also shows that including moist processes leads to new fast-growing structures as indicated by the smaller similarity index between, for example, old1 and new1. Some of the SVs of type new0 and new1 have resemblance to extra-tropical SVs. This may indicate that the target area is probably too far extended in the meridional direction to capture tropical error growth mechanisms. We come back to this in subsection 4.3.

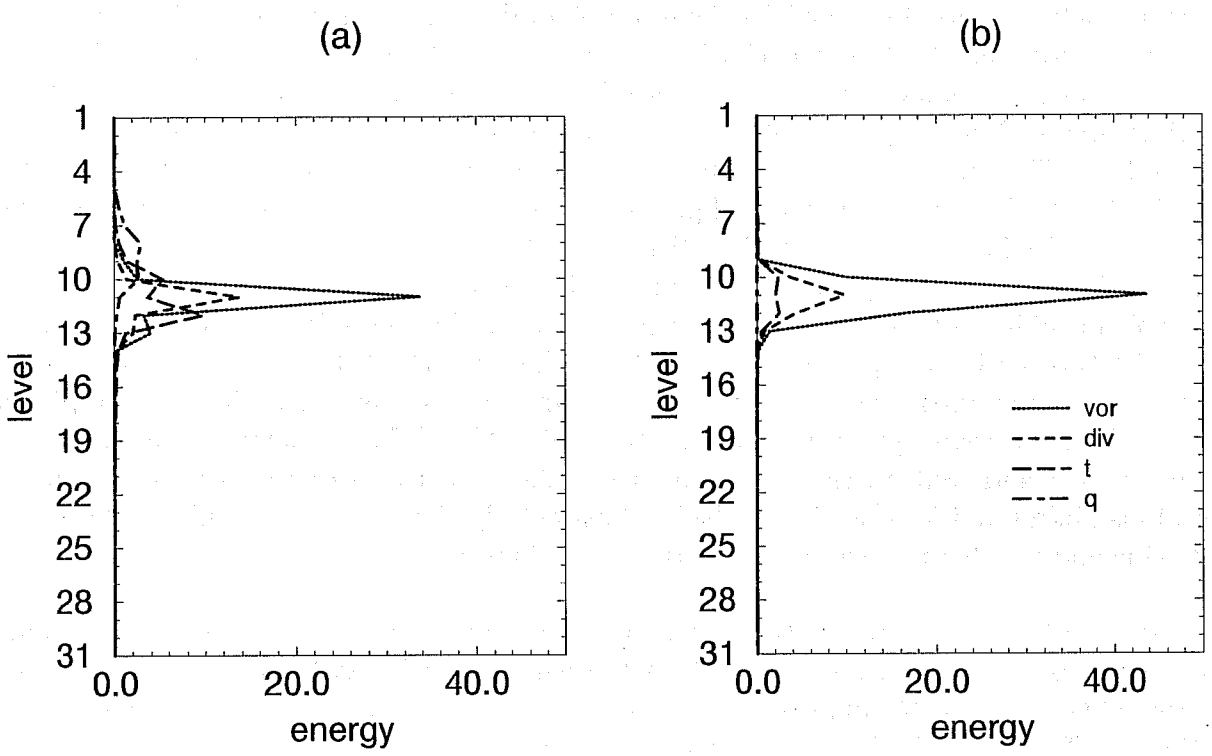

Figure 3: *Vertical distribution of total energy components of SV1 of type new1 for the (a) winter and (b) summer case. Total energy is partitioned into vorticity, divergence, temperature, specific humidity as shown in the right panel.*

4.1 Barotropic and inertial instability

It is not so obvious what physical mechanism is responsible for the structures as displayed in Figs. 2 and 3. It seems that baroclinic instability can be ruled out because of the shallow SV structure and the negligible contribution of available potential energy in the TE-norm at initial time, as given by the temperature component. A possible explanation may be provided by two processes which have been suggested as mechanisms for initiating tropical disturbances:

inertial instability and barotropic instability (Holton 1992; Hunt, 1981). In case of inertial instability, a simple condition for instability in terms of absolute vorticity $\zeta + f$ can be derived. The inertial instability condition states that the flow is unstable in the Northern (Southern) Hemisphere if the absolute vorticity is negative (positive). It is believed that this mechanism triggers unstable perturbations over areas with negative (positive) absolute vorticity in the Northern (Southern) Hemisphere which reduce the lateral shear of the flow until the absolute vorticity is neutral again. A necessary condition for a flow to be barotropically unstable in a region is that the latitudinal gradient of absolute vorticity must vanish somewhere. To see whether the (necessary) conditions for the occurence of these mechanisms for perturbation growth are satisfied, absolute vorticity fields are plotted in Fig. 4. It shows for both the winter and summer case the absolute vorticity in the band 30°S - 30°N of the reference trajectory at initial time for a model level where the SVs attain large amplitude. For the winter case there is a distinct area in Northern Hemisphere (NH) with negative absolute vorticity extending from 60°W - 30°W. The summer case is less clear , but especially the areas 140°W - 20°W and 90°E - 160°E in the SH show quite a number of patches with positive absolute vorticity. It seems that the condition for inertial instability is satisfied for those areas. But, because the latitudinal gradient of the absolute vorticity also changes sign in the same areas it may also be that barotropic instability plays a role in triggering these SVs. Therefore it is not possible to favour one of the two mechanisms for creating the large linear perturbation growth. Nevertheless, the areas indicated above seem important in defining the SVs as can be inferred by plotting the vorticity root-mean-square fields of the 15 leading SVs (of type new1) at model level 11 for the summer and winter case. The locations of the SVs clearly match the areas related to inertial instability and barotropic instability. Particularly the summer case nicely shows both the Pacific and South American area and the Australian area.

To investigate the importance of these areas for the upper-tropospheric SVs, the SV computation with moist TE-norm was repeated for the winter case by excluding 70°W - 50°E from the original target area. No upper-tropospheric SVs were found and the two leading SVs were identical to SV4 and SV5 of new1 (see also section 4.2).

It is likely that these upper-tropospheric SVs are merely an artefact of the linear model, which allows for a growing mechanism absent (or much more damped) in the nonlinear model. To investigate this possible discrepancy between error growth properties of the linear and nonlinear model, SVs (of type new1) were integrated with an initial amplitude comparable to what is used in the ECMWF EPS. The nonlinear evolution changed the vertical structure substantially, as can be concluded from the vertical profile of the total energy distribution. In Fig. 5 the vertical energy distribution is plotted of the various components of the moist TE-norm for the linearly and nonlinearly integrated SV1 of type new1 (winter case). The large growth at the few levels as exhibited by the linearly evolved SV1, is greatly reduced. The contribution of q which is neglible for the linearly evolved SV, now becomes much more pronounced. Reducing the initial amplitude by a factor of 5 gave a similar energy profile for the nonlinearly evolved SV1. Other SVs with not such a shallow vertical structure show a quite good correspondence between linear and nonlinear integrations.

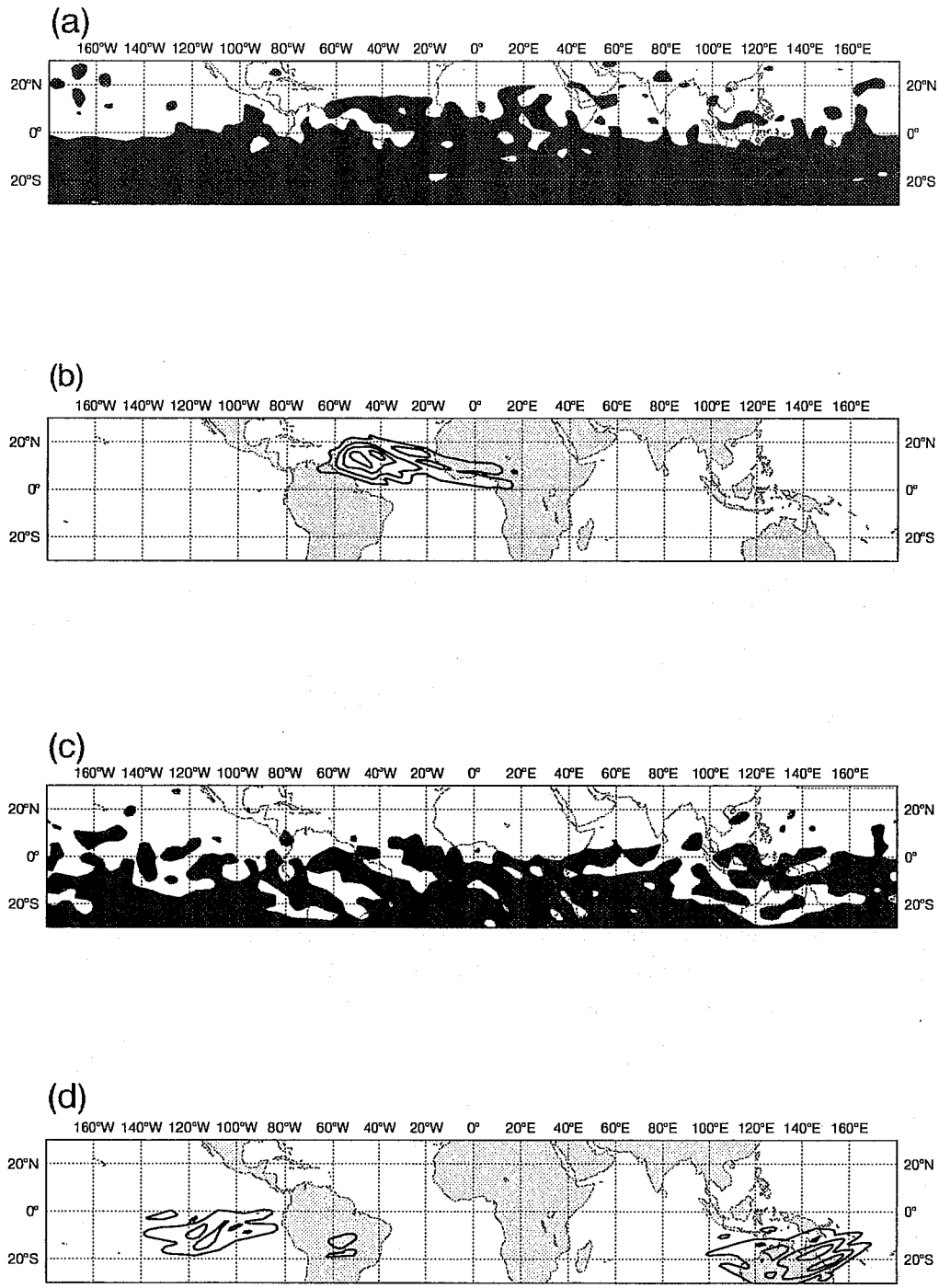

Figure 4: *Absolute vorticity at 238 hPa for (a) 7 February 1997 at 12 UTC and (c) 2 July 1997 at 12 UTC, with positive (negative) values plotted white (black). The corresponding vorticity rms fields of the 15 leading SVs of type new1 for both cases are given in (b) and (d) respectively.*

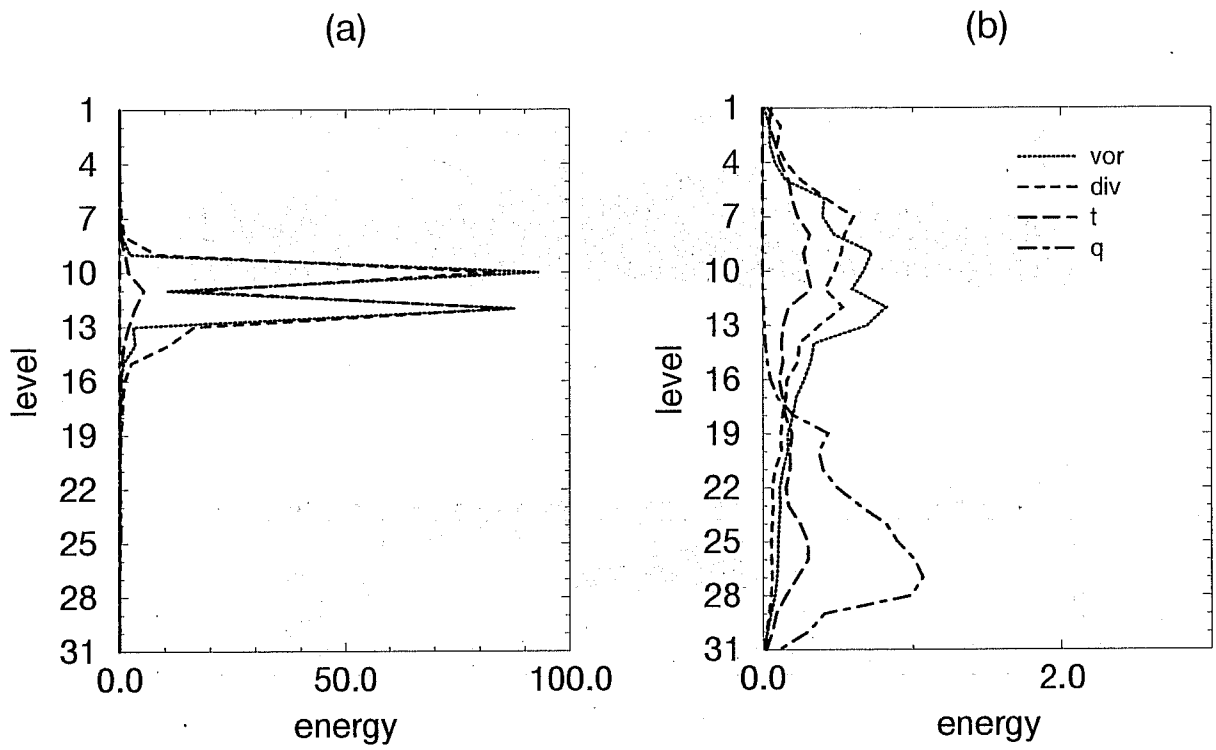

Figure 5: *Energy profiles for SV1 of type new1 (winter case) after (a) linear and (b) nonlinear integrations for 48 hours.*

4.2 Increased vertical diffusion

The fact that the shallow upper tropospheric SVs do not amplify in the nonlinear model indicates that they are not the signature of a genuine meteorological instability of the atmospheric flow. As a consequence, they should not be used to define initial perturbations of the EPS. Various possibilities to avoid the growth of such SVs are examined hereafter.

Strong nonlinearities of the forward model have been identified by Mahfouf (1999) for the wind components in the tropical upper troposphere when examining the accuracy of the tangent linear approximation (see Figure 6 in his paper). The sharp vertical gradients of the shallow SVs can be reduced by applying the linearized vertical diffusion scheme in the upper troposphere. Such increased vertical diffusion can be regarded as an empirical way to account for the nonlinear damping that the linear model cannot describe.

The vertical diffusion scheme in the new linearized physics is based on a K-type closure with exchange coefficients depending on the local Richardson number Ri as descibed in Louis et al. (1982). For any conservative variable ψ (such as wind components u and v, dry static energy

s or specific humidity q), the tendency of its perturbation ψ' as a result of vertical diffusion is (see also Mahfouf (1999)):

$$\frac{\partial \psi'}{\partial t} = \frac{1}{\rho}\frac{\partial}{\partial z}\left(K(Ri)\frac{\partial \psi'}{\partial z}\right) \tag{4}$$

with ρ the air density. In this linearized equation, perturbations of the exchange coefficients are not taken into account: $K' = 0$. The exchange coefficient K is defined as follows:

$$K = l^2 \parallel \frac{\partial \vec{V}}{\partial z} \parallel f(Ri) \tag{5}$$

where $\vec{V} = (u, v)$ is the horizontal wind vector. The mixing length profile $l(z)$ uses the formulation of Blackadar (1962) with a reduction in free atmosphere expressed as:

$$l(z) = \frac{k(z+z_0)}{1+\frac{k(z+z_0)}{\lambda}}\left(\beta + \frac{1-\beta}{1+(\frac{z+z_0}{H})^2}\right) \tag{6}$$

and z_0 is the surface roughness length, k the Von Karman constant and λ an asymptotic mixing length. The current linearized vertical diffusion scheme uses a constant pseudo height of $H = 4000\ m$ for the boundary layer and a reduction factor $\beta = 0.2$ for the asymptotic mixing length in the free atmosphere.

In order to investigate the impact of increased diffusion, SVs were computed with various settings of the pseudo height H and reduction factor β. SVs computed with a linear vertical diffusion setting with $H = 8000\ m$ and $\beta = 2.0$ are denoted by high1 or high0 depending on whether the moist norm is used or not. The two leading SV1 and SV2 of type high1 are identical to SV4 and SV5 of type new1 respectively as computed with the original vertical diffusion scheme ($H = 4000\ m$ and $\beta = 0.2$). Although at initial time, the SVs may still extend throughout the whole depth of the atmosphere, the large amplitudes around model level 10 to 12 are now absent. Singular vectors computed with less diffusion, e.g. $H = 8000\ m$ and $\beta = 1.0$, still have amplitude predominantly in vorticity and divergence and at high model levels. The fit between the linear and nonlinear evolved SVs has improved considerably with the setting $H = 8000\ m$ and $\beta = 2.0$. The amplification factor, defined as the square root of the ratio between the moist TE-norm in the target area of the perturbation at optimization time and the moist TE-norm at initial time, is presented in Fig. 6 for the 10 leading SVs of type new1 and high1 both for linear and nonlinear integrations. Initial amplitudes were comparable to what is used in the ECMWF EPS. Clearly, the amplification factor is affected substantially by the increased diffusion. In particular the leading SVs of type high1 yield comparable linear and nonlinear perturbation growth. Also the vertical energy profiles and spatial patterns of both linear and nonlinear integrations compare well (not shown). On the other hand, the extra-tropical SV computation with new physics is hardly affected by the increased diffusion.

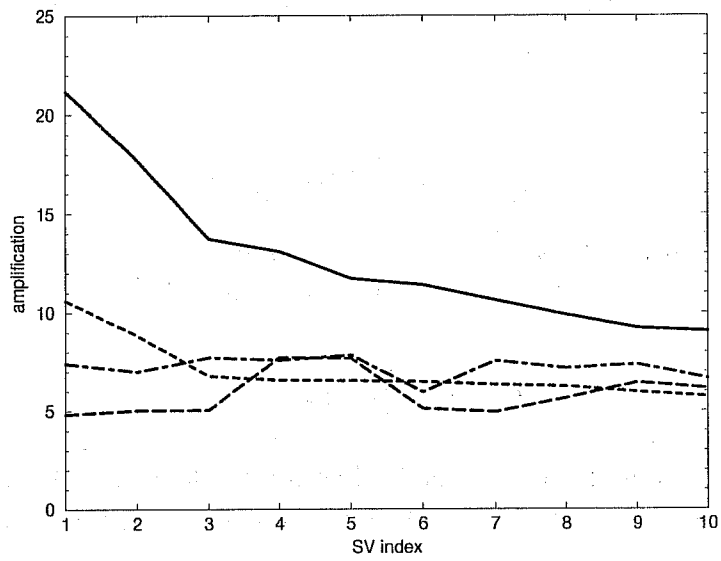

Figure 6: *Total energy amplification of the leading SVs of type new1 (winter case) as given by linear (solid) and nonlinear (long dashed) 2 day integrations and of SVs of type high1 for linear (dashed) and nonlinear (dashed-dot) integrations.*

Table 2 gives the similarity indices between 3 sets of SVs computed with the moist TE-norm and using simplified physics (old1), or new physics with a vertical diffusion scheme with the original parameters $H = 4000\ m$ and $\beta = 0.2$ (new1) or with $H = 8000\ m$ and $\beta = 2.0$ (high1). The use of new physics in the tangent and adjoint models clearly leads to new structures in the subspace spanned by the leading SVs as indicated by the low simililarity index with the SVs computed using simplified physics, see also Mahfouf et al. (1996) and Ehrendorfer et al. (1999). The leading SVs of type new1 yield larger amplification factors than SVs of type old1. By increasing the vertical diffusion as in high1, the amplification becomes similar to SVs of type old1 (not shown).

winter case	old1	new1	high1
old1	1	.48	.5
new1		1	.94
high1			1

Table 2. *Similarity indices between unstable subspaces spanned by the 15 leading extra-tropical SVs based on the moist norm and using simplified (old1) and new physics with the original (new1) and increased (high1) vertical diffusion.*

4.3 Deep tropical singular vectors

The tropical SVs presented thus far were computed with a target area 30°S - 30°N. As a consequence, SVs at initial and optimization time may have substantial amplitude in the extra-tropics at initial and optimization time. An example of this is shown in Fig 7, where streamfunction fields of the 3 leading SVs (of type high1) are plotted at 500 hPa for initial and optimization time. To ensure that the SVs are even more associated with error growth mechanisms present in the tropics, computations were performed with a reduced target area 20°S - 20°N. Unless stated otherwise the vertical diffusion scheme with parameters $H = 8000\ m$ and $\beta = 2.0$ is used. It appears that the choice of target area has a substantial impact on the SV structure. The similarity index between the 15 leading moist SVs for the two target areas is only 0.23. The reduced target area yields SVs with most of the amplitude between 30°S - 30°N at optimization time and SV properties may occur which were not present for the SVs with target area 30°S - 30°N. For instance, the two leading deep tropical moist SVs cannot be described by the original 15 leading moist SVs (of type high1). The vertical energy profiles of these two SVs at initial and final time are shown in Fig. 8. Most of the total energy of SV1 at initial time is in the vorticity and temperature component and confined to the lower model levels (peaking around 800 hPa). At final time, the total energy is dominated by the specific humidity component. This property of transforming all energy in the specific humidity component during the 2 day linear integration occurs for most of the leading moist SVs, but is absent when the dry norm is used. Nonlinear integrations of SV1 show that this energy reversal (Ehrendorfer et al., 1999) is not a result of approximations in the linear models but can also occur for nonlinear evolution of such perturbations. Another SV feature which becomes apparent when computing deep tropical SVs is the vertical distribution of specific humidity at initial time. Fig 8c shows a large amplitude in the q term for SV2 at initial time at high model levels (peaking around 155 hPa) where the atmosphere is very dry.

To reduce the amplitude for q at high levels a modified moist norm for q was used at initial time based on background error covariances, showing an increase in weight above model level 15 (see Fig. 1). Depending on whether or not the original dry or moist norm is used at final time such SVs are denoted by qmod0 or qmod1 respectively. Table 3 gives the similarity indices for various SV configurations. Clearly, use of the modified moist norm has an impact on the unstable subspace. For instance, the experiments high1 and qmod1 have a similarity index of 0.67. Inspection of the unstable subspace of qmod1 shows that, for instance, SVs like SV2 of high1 with q profile shown in Fig. 8a are absent. Both computations high1 and qmod1 yield however several leading SVs with the energy reversal to q as shown in 8c-d. Computations for other cases showed that this property is quite generic for high1 and qmod1 experiments, where q is used in the final norm. Setting the contribution of q in the final norm to zero but allowing amplitude in q at initial time as in qmod0 yields a subspace which is quite similar (similarity index is 0.8) to the subspace obtained in high0 where the q amplitude is also set to zero at initial time. Note that the SVs of qmod0 are not ordered anymore according to their TE amplification as for SVs in high0, because different norms are used at initial and final time.

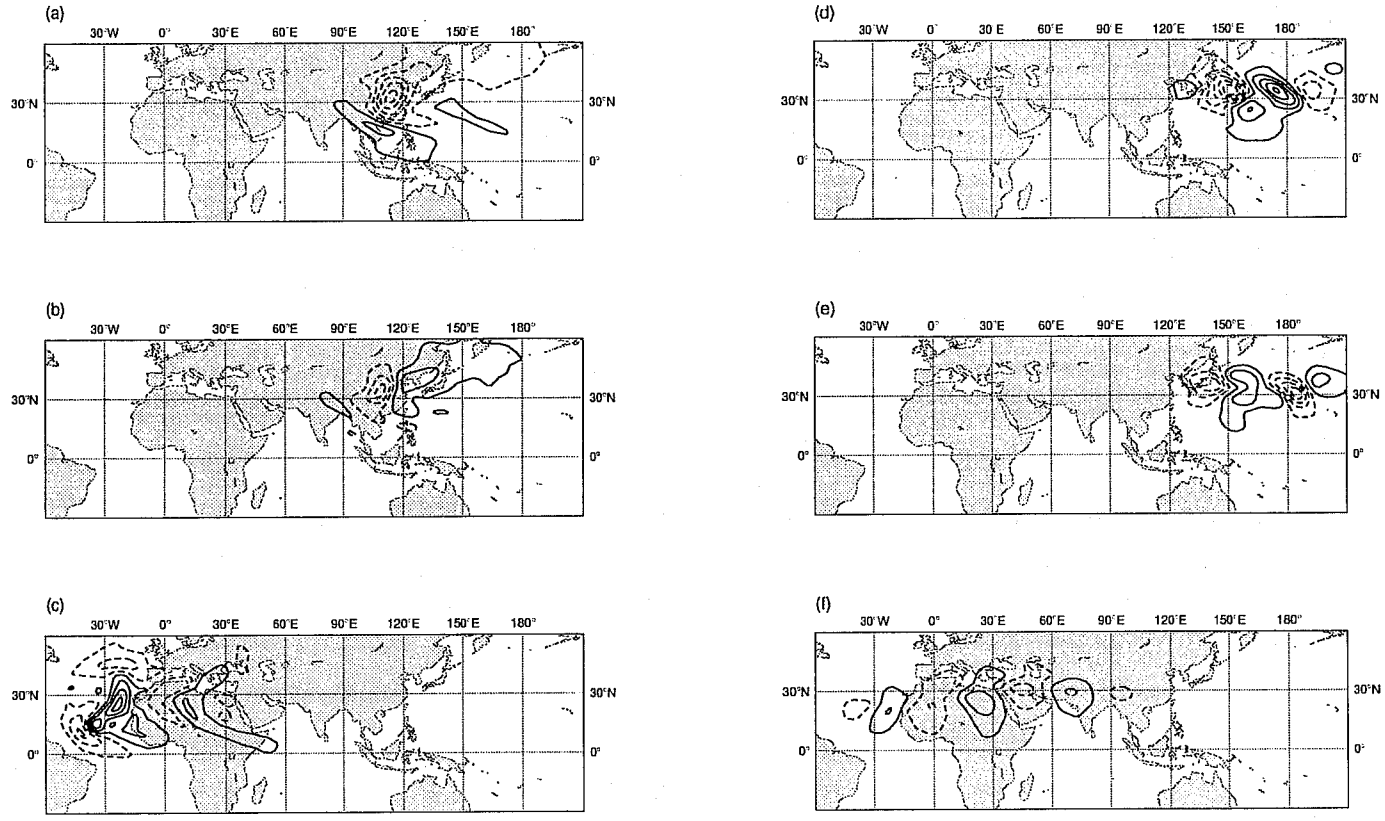

Figure 7: *Streamfunction fields at 500 hPa of the 3 leading SVs (of type high1 and winter case) at (a-c) initial and (d-f) optimization time. The contour interval used in (d-f) is a factor 20 larger as in (a-c).*

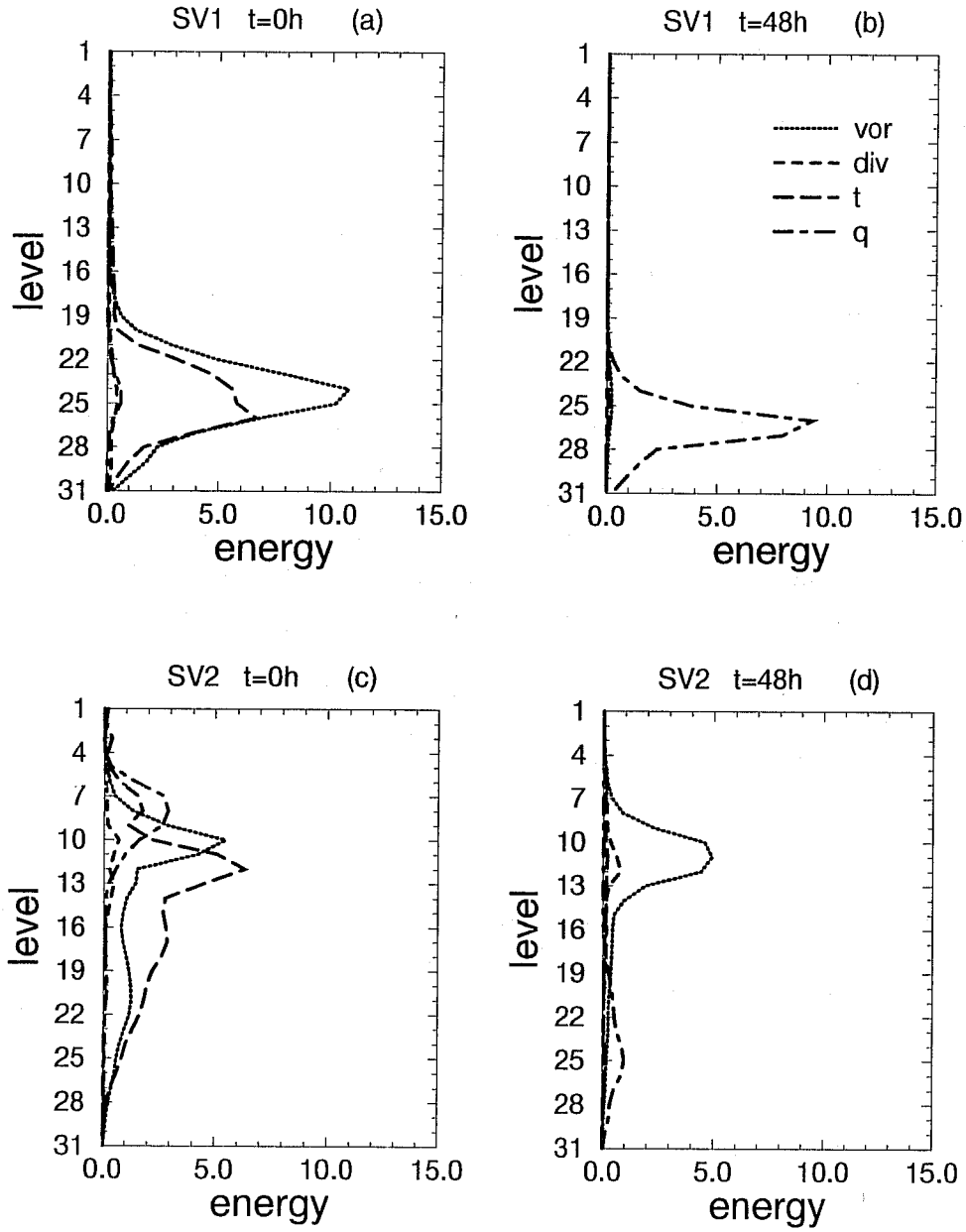

Figure 8: *Energy profiles of the two leading SVs of type high1 (winter case) and targeted for 20°S-20°N at (a,c) initial and (b,d) final time.*

winter case	qmod0	qmod1	high0	high1
qmod0	1	.16	.8	.31
qmod1		1	.16	.67
high0			1	.23
high1				1

Table 3. *Similarity indices between unstable subspaces spanned by the 15 leading tropical SVs for various configurations. The symbol qmod0 or qmod1 denotes that the modified moist norm is used at initial time and the original dry or moist norm at final time.*

Figures 9a,b show the mean energy profiles (averaged over the leading 15 SVs) of qmod0 at initial and final time. The upward propagation of energy as seen in extra-tropical total energy SVs is absent. The energy profiles for high0 are similar but without contribution of q at initial time. The horizontal spectra of qmod0 at initial and final time are given in Figures 9c. Compared to horizontal spectra of extra-tropical SVs there is still the up-scale cascade of energy during two days integrations but there is more energy towards larger scales at initial time (SVs of type high0 give similar results). The streamfunction fields of the 3 leading SVs of qmod0 are given in Fig. 10 at model level 18 (500 hPa). Notice that most of the amplitude is now confined to 30°S - 30°N. We studied whether the SVs for qmod0 could be retained when cumulus convection was switched off in the linear models. The similarity index of 0.64 between the two subspaces consisting of 15 SVs shows that this diabatic process substantially contributes to the structures of the leading SVs.

In the preceding we have seen that spurious shallow SVs in the upper troposphere produced by barotropic and/or inertial instability could be prevented from growing through an increased vertical diffusion in the linearized model. Large values of specific humidity at initial time around 150 hPa have been reduced by replacing the q term in the moist TE norm by a term based on background error statistics. Also mid-latitude SVs can be captured if the tropical area is not restricted enough. These properties of tropical SVs have been useful to design a set-up of targeted SVs for tropical cyclones presented in the next section.

5 Singular vectors targeted for tropical cyclones

As an application of tropical SVs two tropical cyclones, Bonnie and Zeb, were studied, with starting dates 19 August 1998 12 UTC and 11 October 1998 12 UTC respectively. The impact of such SVs on the ECMWF EPS is the subject of a companion paper (Puri et al., 1999). Various SV configurations were tried, varying the choice of final norm and target area. Selecting a

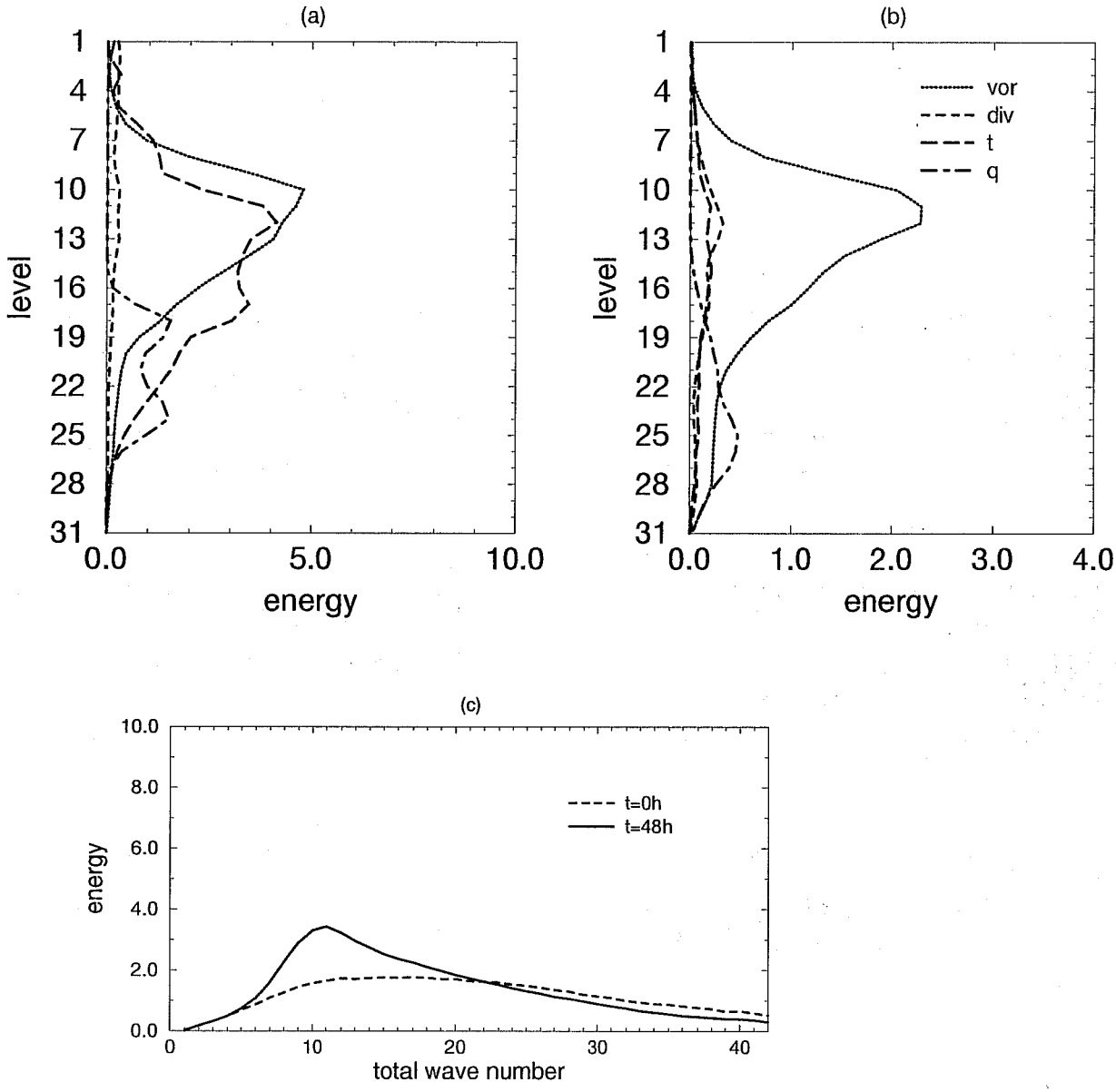

Figure 9: *(a) Initial and (b) final average energy profiles for the 15 leading SVs (of type qmod0 and winter case) and targeted for 20°S-20°N. (c) Corresponding horizontal energy spectra at initial (dashed) and final (solid) time. The energy at initial time is multiplied by a factor of 100.*

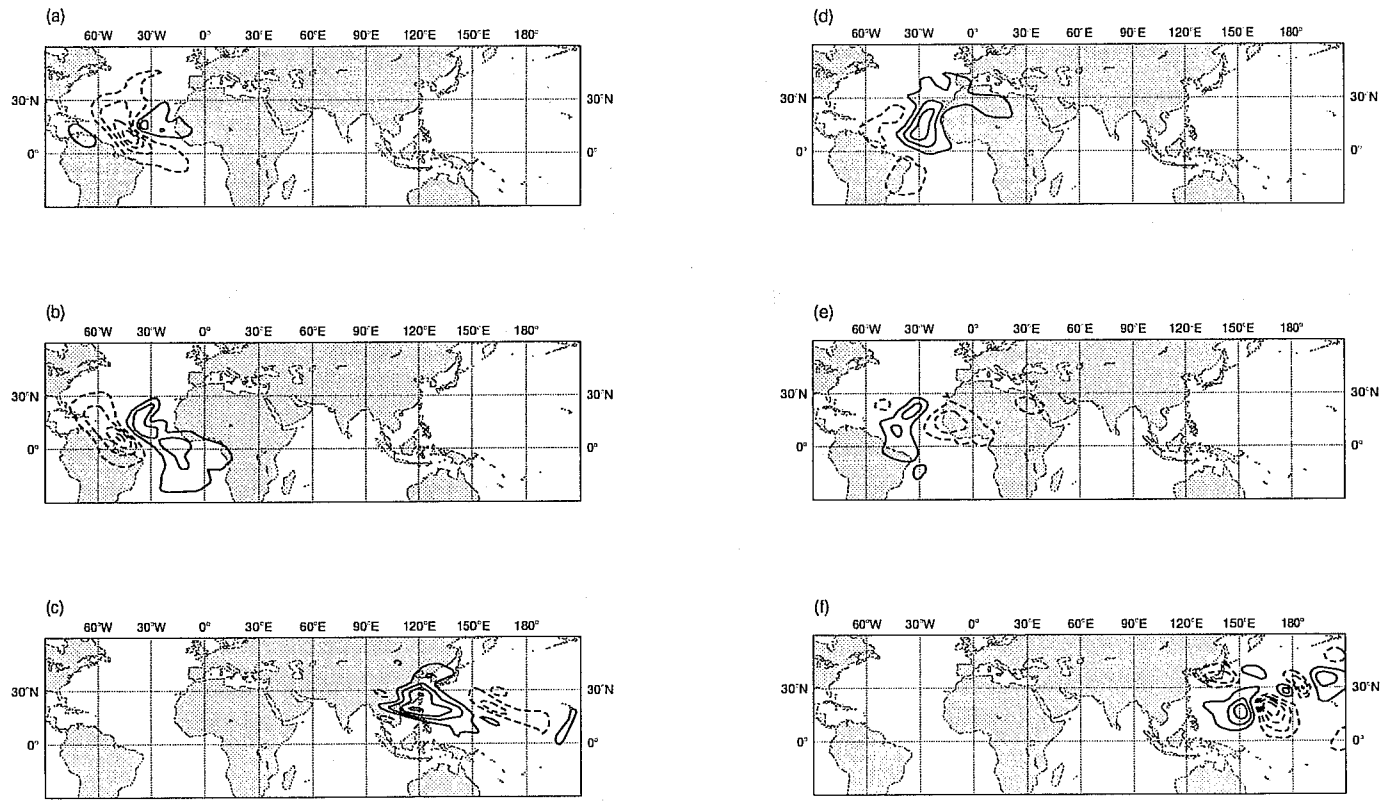

Figure 10: *Streamfunction fields at 500 hPa of the 3 leading SVs (of type qmod0 and winter case) and targeted for 20°S-20°N at (a-c) initial and (d-f) final time. Contour interval at final time is a factor 10 larger than used at initial time.*

target area in the vicinity of the forecast cyclone track up to optimization time makes it more likely that SVs are associated with cyclone development. Target areas used for Bonnie and Zeb were, for example, 10°N - 30°N, 80°W - 60°W and 0°N - 30°N, 110°E - 140°E respectively. As noted in section 4.1, SV computations without increased vertical diffusion lead to SVs with spuriously large perturbation growth in the upper-troposphere. This also appeared to be the case for the targeted SVs. Since perturbation growth for these SVs is only confined to a few model levels, targeted SV computations were performed with a final norm set to zero above model level 18 (500 hPa) but without increased vertical diffusion. Similarity indices based on 25 initial SVs with the dry TE norm showed a good correspondence with the SVs obtained with the increased vertical diffusion setting high0 (0.76 and 0.79 for Bonnie and Zeb respectively). The use of simplified or new physics in the linear models became noticeble in nonlinear integrations of SVs: those computed with new physics better survived integration with the nonlinear dynamics and contributed to larger perturbation growth (not shown). This may partly explain why new physics SVs when applied in ensemble forcasting produce larger spread in cyclone track positions than SVs using simplified physics (see Puri et al., 1999). The SV computations reported hereafter use new physics in the linear models together with the vertically capped final TE norm and only the dry version. Including the specific humidity q–term in the TE norm at final time again resulted predominantly in SVs with all energy in q at final time, as with SV computations of type high1 or qmod1. Based on ensemble results, where such moist SVs showed little impact on circulation fields, it was decided to leave the q-term from the TE-norm.

The choice of the target area is crucial in determining the locations and properties of SVs (see also section 4.3). Selecting as target area the whole tropical strip 20°S - 20°N resulted in many SVs which were not located in the cyclone area: similarity indices based on the first 25 initial SVs were only 0.05 and 0.01 for Zeb and Bonnie respectively. Only SV12 and SV13 for the Zeb case and computed with the 20°S - 20°N target area had some projection on SV2 of the SVs computed for the smaller target area 0°N - 30°N, 110°E - 140°E. The SVs computed with a target area 30°S - 30°N even resulted in smaller similarity indices. Figure 11 shows the SV locations at initial time for Bonnie and Zeb and both tropical strip target areas as given by the streamfunction root-mean-square fields of the leading 25 SVs. This critical dependence of the SV location on the target area shows that if tropical SVs are considered for hurricane ensemble prediction in an operational environment, the target area should be chosen with some care. To explore the sensitivity of SVs to the target area we therefore determined also SVs by targeting on the area where cyclones are likely to occur. For the Atlantic and Pacific region the selected target areas are 100°W - 0°W, 0°N - 30°N and 100°E - 220°E, 0°N - 30°N respectively. Similarity indices of 0.68 and 0.77 between the smaller target area and the Atlantic and Pacific (based on 25 SVs) region show that the unstable subspace has changed. However, the impact of both sets on the ensemble performance is quite similar, see Puri et al. (1999). This in contrast to the SVs computed for the tropical strip, which resulted, for instance, in a much reduced spread for the cyclone tracks. Based on additional experiments it does not seem necessary to choose a target area in the close neighbourhood of the cyclone location. A target area which encompasses the preferred cyclone locations in the Atlantic and Pacific cyclone season is sufficient.

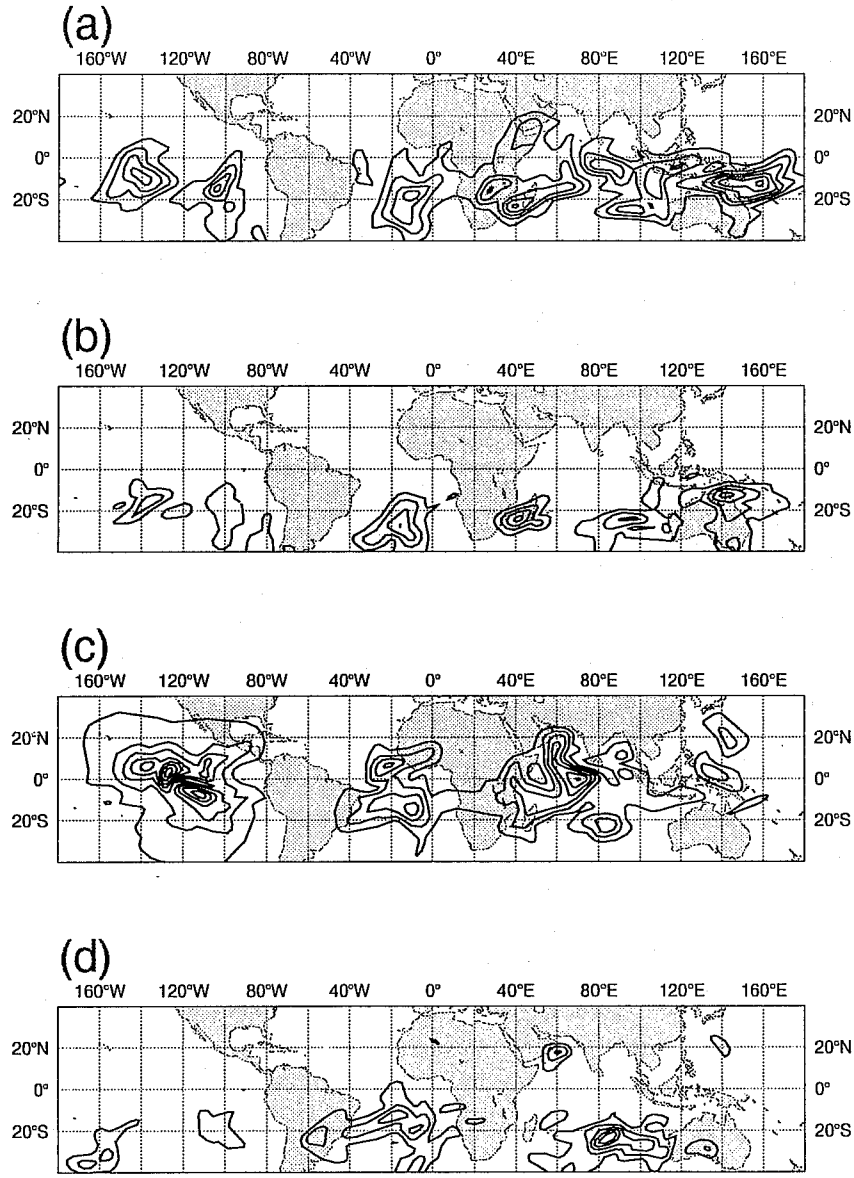

Figure 11: *Streamfunction rms fields of the leading 25 SVs for tropical cyclone Bonnie and targeted for (a) 20°S-20°N and (b) 30°S-30°N ; (c-d) same as (a-b) but for tropical cyclone Zeb.*

For the two smaller target areas for Zeb and Bonnie, as mentioned above, T63 SVs were also determined. Figures 12 and 13 show the 2 leading SVs for the T42 and T63 computations at three model levels in case of Zeb. Clearly, there are similarities between the two sets (similarity indices based on 25 SVs are 0.53 and 0.65 for Bonnie and Zeb respectively). The T42 and T63 SVs had a comparable impact on the EPS performance for both cyclone cases (Puri et al., 1999). It is worth pointing out that in particular the leading T63 SVs show resemblance to spiraling optimal perturbations found by Nolan and Farrell (1999) for idealized vortices.

In the case of tropical cyclone Bonnie (19 August 1998), the need for targeting seems to be the result of a more unstable Southern Hemisphere (SH) winter circulation. Computations with target area 30°S - 30°N and 20°S - 20°N, yield SVs which are mainly located in the SH, see Figure 11a,b. To see whether tropical cyclone Bonnie could be isolated as an important feature without unnecessarily restricting the SV location, the tropical strip 0°N - 20°N was selected as target area. Figure 14 shows the streamfunction root-mean-square fields of the leading 25 SVs. Clearly all leading SV are now predominantly located in the NH and tropical cyclone Bonnie in the Atlantic area is now covered well by SVs. Observe that also other areas associated with perturbation growth are now selected by the SV computation such as the monsoon area in the North Indian Ocean and the western African area, where so-called easterly waves originate. Figure 15 shows an example of a westward propagating SV at 500 hPa located over western Africa, together with the wind vector fields of the basis state.

6 Conclusions

The development of a set of linear physical parametrizations for the tangent-linear and adjoint model versions of the ECMWF global forecast model as described in Mahfouf (1999) makes it possible to compute SVs for situations where physical processes may play an important role in perturbation growth. In this study we focused on the tropical region and determined tropical SVs exploring different norm configurations. For instance, the impact of including specific humidity in generating perturbation growth was studied.

First experiments with the new set of linear parametrizations resulted in SVs which had very shallow structure. Similar SVs were found with the original tangent and adjoint model which only uses a simplified vertical diffusion scheme (Buizza, 1994). Most of the energy was confined to a few (upper-tropospheric) model levels and dominated by the vorticity and divergence. Moreover, the linear and non-linear evolution of these SVs showed a large discrepancy between their spatial pattern and perturbation growth. There is indication that these SVs are caused by inertial instabilities which are allowed to amplify freely in the linear model. For this reason the standard setting for the pseudo height of the boundary layer and for the asymptotic mixing length in the free atmosphere were changed to increase the vertical diffusion in the linear

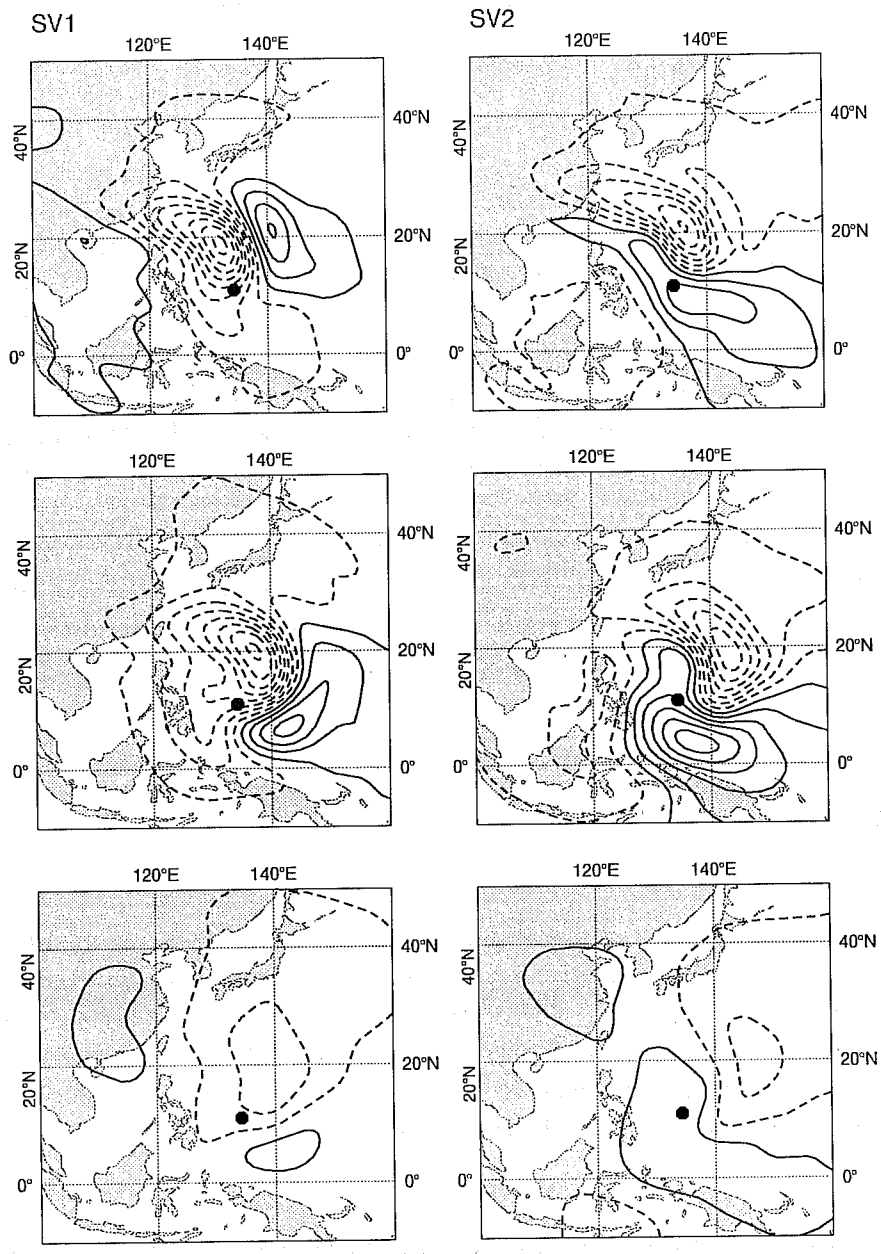

Figure 12: *Streamfunction fields of the 2 leading SVs for tropical cyclone Zeb at 3 model levels (155 hPa, 500 hPa and 770 hPa from top to bottom panel). The cyclone location is indicated by a large dot.*

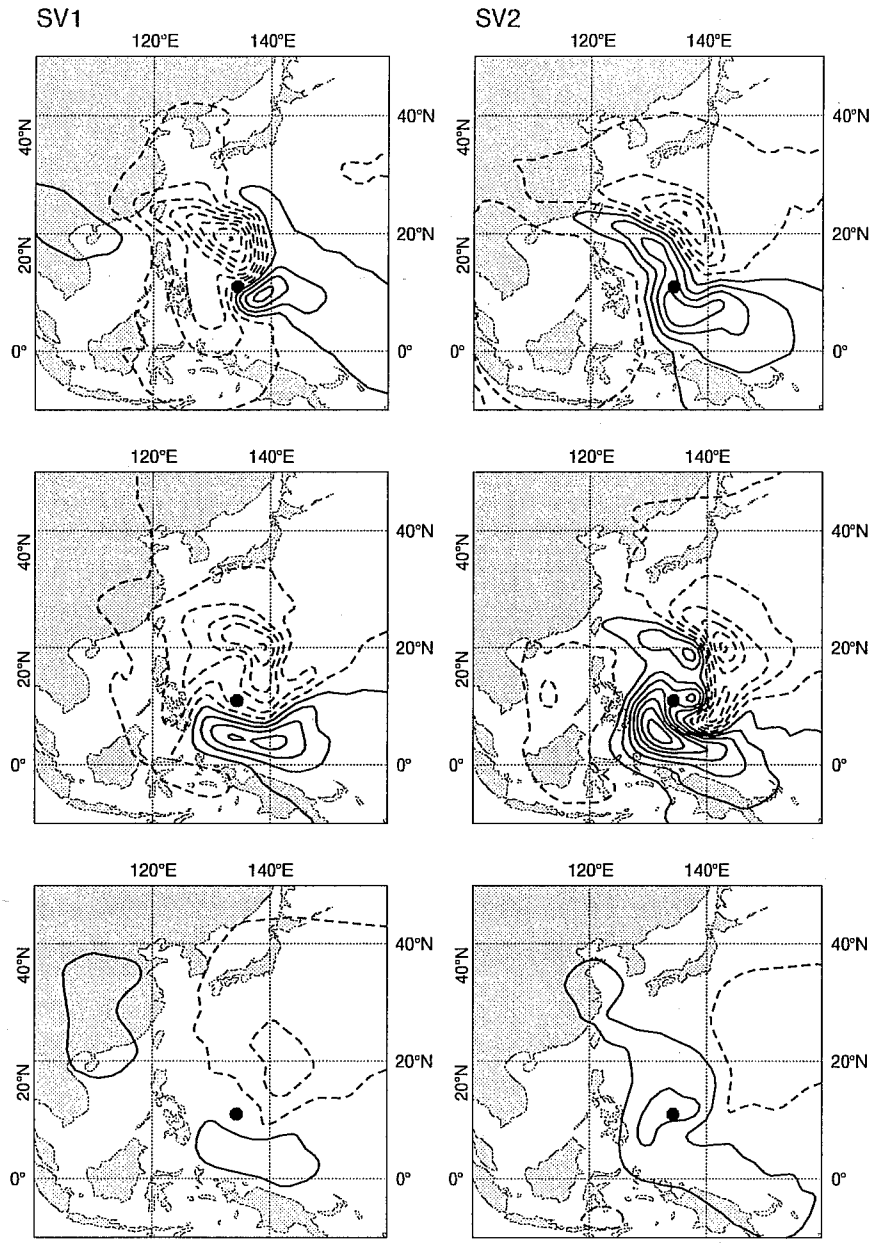

Figure 13: *Same as figure 12 but for SV1 and SV2 computed at truncation T63.*

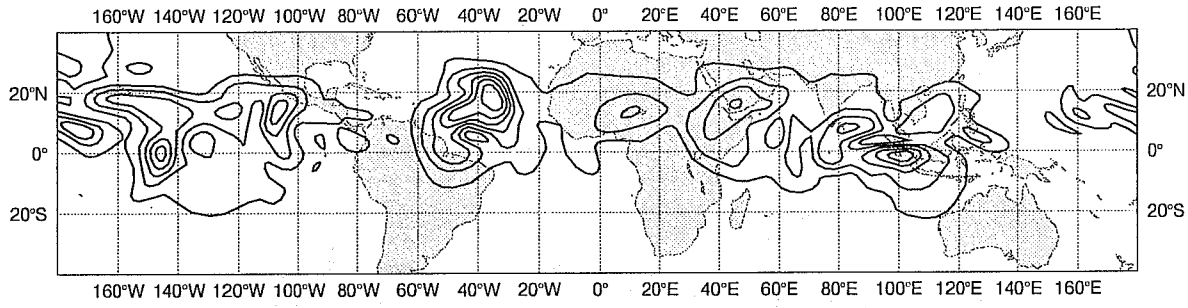

Figure 14: *Streamfunction rms field of the leading 25 SVs for tropical cyclone Bonnie and targeted for 0°N-20°N.*

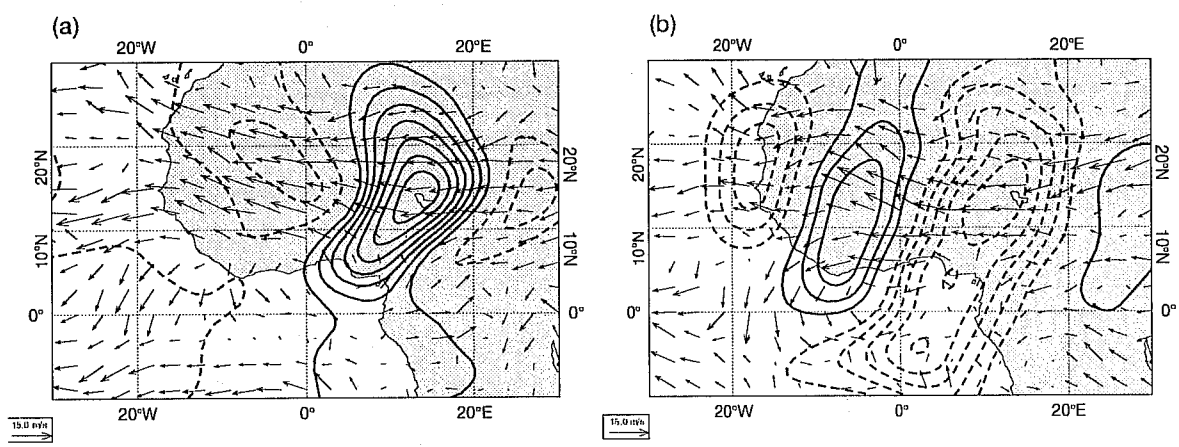

Figure 15: *Streamfunction fields at 500 hPa of a westward propagating SV at (a) initial and (b) final time, with the wind vector fields of the corresponding analyses. Contour interval used in (b) is a factor 3 larger than in (a).*

models at higher model levels. This prevented the occurrence of these shallow SVs. Moreover, the linear and nonlinear SV integrations showed a better match. In the extra-tropics, where the perturbation growth is dominated by baroclinic processes, the SVs are not affected by the increased vertical diffusion.

For two tropical cyclone cases in 1998, namely Bonnie and Zeb, targeted SVs were determined in various configurations. Results show that the selection of a target area requires some care in order to pick up perturbation growth associated with cyclone evolution. In a companion paper (Puri at al, 1999), the impact of these targeted tropical singular vectors on the performance of the ECMWF Ensemble Prediction System will be studied. One of the findings is that including linearized diabatic physics in the singular vector computation has a noticeble impact on the spread in cyclone tracks.

7 Acknowledgements

Drs A. Simmons and M. Miller are thanked for giving comments on an earlier version of the manuscript.

8 References

Barkmeijer, J., Gijzen, Van M., and F. Bouttier, 1998: Singular vectors and estimates of the analysis error covariance metric. *Quart. J. Roy. Meteor. Soc.*, 124, 1695-1713.

Blackadar, A.K., 1992: The vertical distribution of wind and turbulent exchange in a neutral atmosphere.*J. Geophys. Res.*, 67, 3095-3102.

Buizza. R. and T.N. Palmer, 1995: The singular vector structure of the atmospheric general circulation. *J. Atmos. Sci.*, 52, 1434-1456.

Buizza, R., 1994: Sensitivity of optimal unstable structures. *Quart. J. Roy. Meteor. Soc.*, 120, 429-451.

Buizza, R., Palmer, T.N., Barkmeijer, J., Gelaro, R. and J.-F. Mahfouf, 1996: Singular vectors, norms and large-scale condensation. 11th Conference on Numerical Weather Prediction, Norfolk, Virginia, American Meteorological Society, 50-52.

Derber, J. and F. Bouttier, 1999: A reformulation of the background error covariance in the ECMWF global data assimilation system. *Tellus,* **51A,** 195-222.

Ehrendorfer, M. and J.J. Tribbia, 1997: Optimal prediction of forecast error covariances through singular vectors. *J. Atmos. Sci.*, 54, 286-313.

Ehrendorfer, M., Errico, R.M., and K.D. Reader, 1999: Singular vector perturbation growth in a primitive-equation model with moist physics. *J. Atmos. Sci.*, 56, 1627-1648.

Errico, R.M. and K.D. Reader, 1999: An examination of the accuracy of the linearization of a mesoscale model with moist physics. *Quart. J. Roy. Meteor. Soc.*, 125, 169-195.

Gelaro, R., Buizza, R., Palmer, T.N., and E. Klinker, 1998: Sensitivity analysis of forecast errors and the construction of optimal perturbations using singular vectors. *J. Atmos. Sci.*, 55, 1012-1037.

Holton, J.R., 1992: An introduction to dynamic meteorology. International Geophysics Series Vol. 23. Academic Press.

Hunt, B.G., 1981: The maintenance of the zonal mean state of the upper atmosphere as represented in a three-dimensional general circulation model extending to 100 km. *J. Atmos. Sci.*, 38, 2172-2186.

Lorenz, E.N., 1965: A study of the predictability of a 28-variable atmospheric model. *Tellus*, 17, 321-333.

Lorenz, E.N., 1982: Atmospheric predictability experiments with a large numerical model. *Tellus*, 34, 505-513.

Louis, J.-F., Tiedtke, M., and J.-F. Geleyn, 1982: A short history of the operational PBL parametrization at ECMWF. In *ECMWF Worksshop on boundary layer parametrization*, pages 59-79, November 1981, ECMWF, Shinfield Park, Reading, RG2 9AX, UK.

Mahfouf, J.-F., Buizza, R., and R.M. Errico, 1996: Strategy for including physical processes in the ECMWF variational data asimilation system. In *ECMWF Workshop on non-linear aspects of data assimilation*, pages 595-632, 9-11 September 1996, ECMWF, Shinfield Park, Reading, RG2 9AX, UK.

Mahfouf, J.-F., 1999: Influence of physical processes on the tangent-linear approximation. *Tellus*, 51A, 147-166.

Mahfouf, J.-F. and F. Rabier, 1999: The ECMWF operational implementation of four dimensional variational assimilation, Part II: experimental results with improved physics. ECMWF, Technical Memorandum No 242, 26pp. Available from ECMWF, Shinfield Park, Reading RG2 9AX, UK.

Molteni, F. R. Buizza, T.N. Palmer and T. Petroliagis, 1996: The ECMWF ensemble prediction

system: methodology and validation. *Quart. J. Roy. Meteor. Soc.*, 119, 269-298.

Nolan, D.S. and B.F. Farrell, 1999: Generalized stability analyses of asymmetric disturbances in one- and two-celled vortices maintained by radial inflow. *J. Atmos. Sci.*, 56, 1282-1307.

Palmer, T.N., R. Gelaro, J. Barkmeijer and R. Buizza, 1998: Singular vectors, metrics and adaptive observations. *J. Atmos. Sci.*, 55, 633-653.

Puri, K., Barkmeijer, J. and T.N. Palmer, 1999: Ensemble prediction of tropical cyclones using targeted diabatic singular vectors. ECMWF, Technical Memorandum No 298. Available from ECMWF, Shinfield Park, Reading RG2 9AX, UK.

Parlett, P., 1980: The symmetric eigenvalue problem. Series in computational mathematics. Prentice Hall, New Jersey, USA, 348pp.

Rabier, F., E. Klinker, P. Courtier and A. Hollingsworth, 1996: Sensitivity of forecast errors to initial conditions. *Quart. J. Roy. Meteor. Soc.*, 122, 121-150.

Rabier, F., Mahfouf, J.-F., Fisher, M., Järvinen, H., Simmons, A., Andersson, E., Bouttier, F., Courtier, P., Hamrud, M., Haseler, J., Hollingsworth, A., Isaksen, L., Klinker, E., Saarinen, S., Temperton, C., Thépaut, J.-N., Undén, P., Vasiljević, D., 1997: Recent experimentation on 4D-Var and first results form a simplified Kalman filter. ECMWF, Technical Memorandum No 240, 42pp. Available from ECMWF, Shinfield Park, Reading RG2 9AX, UK.

Simmons, A.J., Mureau, R., and T. Petroliagis, 1995: Error growth and estimates of predictability from the ECMWF forecasting system. *Quart. J. Roy. Meteor. Soc.*, 121, 1739-1771.

Thépaut, J.-N., and P. Courtier, 1991: Four dimensional variational assimilation using the adjoint of a multilevel primitive equation model. *Quart. J. Roy. Meteor. Soc.*, 117, 1225-1254.

Vukićević, T., and R.M. Errico, 1993: Linearization and adjoint of parametrized diabatic processes.*J. Tellus.*, 45A, 493-510.